Chemical Engineering Science 315 (2025) 121877

Contents lists available at ScienceDirect

Chemical Engineering Science

journal homepage: www.elsevier.com/locate/ces

Role of activation progress on textural properties of biochar and their impact on tar cracking

Wadii Arayedh [a], Laurent Van de Steene [b], Khashayar Saleh [a], Elias Daouk [a,*]

[a] University of Technology of Compiègne, ESCOM, TIMR (Integrated Transformations of Renewable Matter), Research center Royallieu – CS 60 319-60 203 Compiègne Cedex, France
[b] BioWooEB, University of Montpellier, CIRAD, Montpellier, France

ARTICLE INFO

Keywords:
Biochar
Activation progress
Specific surface area
Pore size distribution
Tar conversion

ABSTRACT

The gasification process converts biomass into syngas and produces biochar, a porous solid by-product, potentially with a high surface area, ideal for tar cracking applications. In this study, biochars with varying textural properties were produced by activating them under CO_2 and H_2O atmospheres to different extents of conversion. The relationship between these properties—particularly surface area and pore size distribution—and the conversion of a model tar was then examined.

Results show that while the activation agent (CO_2 or H_2O), which impacts pore size distribution, had minimal influence on tar conversion, the activation progress, controlling specific surface area, was crucial. At 850 °C, toluene conversion ranged from 35 % for biochar with 300 m^2/g surface area to nearly 100 % for biochar with 800 m^2/g. Additionally, activation improved gas quality, with higher concentrations of H_2, CO, and CH_4 correlating with increased biochar surface area.

1. Introduction

Pyrogasification is a thermochemical process involving the conversion of biomass or waste into syngas, mainly carbon monoxide (CO), hydrogen (H_2) and methane (CH_4). Solid residue known as biochar is also produced during pyrogasification, which potentially presents an economic potential. Biochar is made up of carbon (80–90 %) and traces of oxygen, nitrogen, hydrogen and various mineral species. The physicochemical properties of biochars, including their textural characteristics, are strongly influenced by the origin of the biomass and the operating conditions of production (temperature, heating rate, pressure, atmosphere, etc.). Porosity of biochars (microporous and mesoporous structures), and specific surface areas are of great interest for many applications. Physical activation of lignocellulosic materials under steam, carbon dioxide, air, or a mixture of these gases can sometimes be used to enhance the porous structure and produce activated carbons with a variety of pore size distributions (Rodríguez-Reinoso et Molina-Sabio 1992). Physical activation under CO_2 develops micropores, while steam generates activated chars with a mesoporous part in their structure (Mohamed, Mohammadi, et Darzi 2010). In addition to their porous structure, biochars contain active sites on their surface, which may include transition metal species (alkali and alkaline earth metals), oxygen functional groups, such as acidic lactols, lactones, phenolic and carboxylic groups, or basic carbonyls and quinones (Boehm et al. 1964). Depending on their properties, biochars can be used as adsorbents for the separation and removal of unwanted substances from industrial effluents, gas and wastewater treatment (Wong et al. 2018), or for soil amendment (Hilber et Bucheli 2013). Biochars can also be used as catalysts or as catalyst supports (Iwanow et al. 2020), for biodiesel synthesis via transesterification of palm fatty acid distillate (Hazmi et al. 2025), triglycerides (Dhawane et Halder 2019), or algale (İnan, Koçer, et Özçimen 2023). Biochars have also proven to be efficient in catalysing tar cracking reactions. for tar cracking. Many studies in the literature have investigated the catalytic cracking of toluene, a model tar compound, on biochars. Toluene belongs to the family of light, single-ring aromatics, which are the main tars produced by the gasification of biomass and wastes, accounting up to 60 % of the total tar content (Coll et al. 2001; Milne, Evans, et Abatzaglou 1998). Catalytic cracking of tars in the presence of a biochar is a promising option, both technically and economically, as biochars have shown excellent catalytic potential for this purpose. Catalytic cracking converts tar molecules into high value-added gases at lower temperatures (< 900 °C) than those required for thermal cracking (1200 °C). In fact, high specific surface area potentially implies higher catalytic activity for tar conversion. Wang et al. (Wang

* Corresponding author.
E-mail address: elias.daouk@utc.fr (E. Daouk).

https://doi.org/10.1016/j.ces.2025.121877
Received 13 January 2025; Received in revised form 9 May 2025; Accepted 16 May 2025
Available online 18 May 2025

et al. 2014) observed that the activated char catalyst exhibited much better catalytic performance for tar reduction than unactivated char. Similar results were reported by Nestler et al. (Nestler et al. 2016) for naphthalene decomposition. Bhandari et al. (Bhandari et al. 2014) showed that activated carbons were more efficient at removing toluene than biochar catalysts. This increased efficiency of activated carbon catalysts is attributed to their significantly larger surface area (900 m^2/g compared to less than 10 m^2/g for biochar). De Caprariis (de Caprariis et al. 2020) demonstrated that the tar abatement capacities were highly influenced by the surface area of the catalytic material, and a linear correlation was found between the area of the catalytic material exposed to tar and the amount of converted tar. Shen and Yoshikawa (Shen et Yoshikawa 2013) stated that the highly porous textural structures of the activated carbons or charcoals (derived from biomass or coal) would improve the dispersion of metal ions on the carbon structure. The macropores and mesopores of these materials would also facilitate the transport of reactant molecules (e.g., toluene, 0.68 nm molecular size) into the internal surfaces of the catalyst. However, the role of pore size distribution in the tar cracking mechanism still not fully understood. Fuentes-Cano et al. (Fuentes-Cano et al. 2013) showed that the initial internal structure of the chars did not affect the initial conversion rate of tars, before deactivation. These conclusions were drawn from studies on various materials, including bio-based chars, coals, and mineral catalysts (i.e. Al_2O_3, pumice and olivine).

To summarize, numerous studies in the literature have enhanced our understanding of the role of biochar's textural properties in the cracking of tars. These studies often compared biochars from different feedstocks, each possessing distinct properties. However, this approach has a limitation: the biochars originated from diverse feedstocks, which introduced variations in both properties and composition, complicating the interpretation of the specific influence of textural properties.

Thus, the primary objective of this study was to produce and comprehensively characterize biochars that differ exclusively in their textural properties. To achieve this, we activated beechwood-derived charcoal under varying activation progress and reactive atmospheres, demonstrating that the textural properties can be controlled through adjustment of operating conditions. The second objective was to investigate the effect of these textural properties, specifically the initial specific surface area and pore size distribution on the conversion of a model tar.

We believe these results will be valuable for advancing the understanding of the relationship between activation conditions, textural properties, and tar cracking performance of activated biochar, providing key insights for optimizing biochar for specific industrial applications.

2. Materials and methods

2.1. Precursor material

Biochars were produced from beech wood, whose characteristics are listed in Table 1. Beech wood particles with a diameter in the range of 1.8–2.5 mm were selected for the experiments. The high carbon and low ash content make beech wood an ideal starting material for the production of activated biochars.

Table 1
Proximate and ultimate analysis of the raw beech wood and biochar (% dry basis, d.b.).

	Proximate analysis (%d.b.)			Ultimate analysis (%d.b.)			
	Volatile Matter	Ash	Fixed Carbon*	C	H	N	O*
Beech wood	84.7	0.8	14.5	45.7	5.7	0.3	47.5
Raw biochar	6.6	3.1	90.3	92.8	0.6	0.3	3.2

*by difference.

2.2. Preparation of activated biochars

The activated biochars were prepared in two steps. Firstly, a fixed-bed pyrolysis reactor at 900 °C was used to produce raw biochar from beech wood with a particle size of 1.8–2.5 mm under an inert atmosphere (N_2). The wood sample was heated at a rate of 5 K/min to the final temperature of 900 °C, and held at the temperature for 1 h a. The resulting biochar was then activated either at 900 °C in a 20 %vol CO_2 atmosphere or at 800 °C in a 20 %vol H_2O one. Instead of pure CO_2 or H_2O, a gas mixture of CO_2/N_2 or H_2O/N_2 (20/80 %vol) was used in the present study to ensure a homogeneous activation in the longitudinal direction of the biochar bed. The use of this same gas mixture composition is also reported and discussed in the literature (Tagutchou et al. 2013).

Activated biochars were produced with varying activation conversion progresses, ranging from 15 % to 85 %, by controlling the activation duration. The objective of this preparation process was to produce activated biochars with different textural properties to study their role in tar cracking. The equipment and methods used for this process are detailed in the following sub-sections.

2.2.1. Carbonisation

Wood carbonization was done in a fixed bed reactor designed to produce batches of homogenous biochars. Three kilograms of beech wood were divided into 10 samples, each placed on a steel plate (i.d. 24 cm), which were then heated in a tubular resistance furnace as described elsewhere (Dufourny et al. 2019). This configuration ensures homogeneous biochar production during pyrolysis. The use of multiple plates achieves more uniform temperatures within the solids during pyrolysis process. A nitrogen flow rate of 5 Nl/min continuously sweeps the reactor, maintaining an inert atmosphere for pyrolysis. The wood samples were heated at a rate of 5 K/min to a final temperature of 900 °C, where they were held for 1 h. The high pyrolysis temperature was chosen to ensure the release of most of the volatile compounds. The low heating rate ensures uniform temperature across the wood particles, resulting in a biochar that is relatively homogeneous from both a structural and chemical point of view (Mermoud, Salvador, et al. 2006; Henriksen et al. 2006; Pattanotai, Watanabe, et Okazaki 2013). After pyrolysis, the furnace was cooled to room temperature in a nitrogen atmosphere. The characteristics of the raw biochar are listed in Table 1. As expected, more than 90 %d.b. of the material was fixed carbon, with an ash content of approximately 3 %d.b. Energy dispersive X-ray (EDX) microanalysis revealed the presence of calcium (Ca), potassium (K), magnesium (Mg) and aluminium (Al) in the raw biochar.

2.2.2. Physical activation

Raw biochar resulting from carbonisation was activated in a reactive atmosphere consisting of 20 % CO_2 or H_2O diluted in N_2. The physical activation was carried out in a vertical fixed-bed reactor placed in an electric furnace (Huchon et al. 2024). The activation reactor used for this study (Fig. 1 (a)) is a refractory steel tube with an internal diameter of 41.9 mm. An empirical rule suggests that radial variations in fluid velocity, porosity, and dispersion coefficient can be neglected when the ratio of the reactor's internal diameter (D) to the particle diameter (d) is greater than 15 ($D/d > 15$). Under these conditions, the flow can be approximated as one-dimensional, corresponding to ideal plug flow behaviour (Korus, Samson, et Szlęk 2020). The reactor outlet is connected to a sampling train to analyse the gases exiting the reactor with a micro chromatography analyser. The activation gas (CO_2 or H_2O in N_2) was preheated by passing through a 4 mm tube inside the furnace and injected at the top of the reactor at a flow rate of 10 Nl/min. To control the steam flow rate, liquid water was fed to a mass flow rate controller before being vaporised in the activation reactor. A biochar fixed bed of approximately 7 g, supported by a grid, was placed in the isothermal zone in the middle of the reactor. Physical activation occurred as the reactive gas passed through the biochar bed.

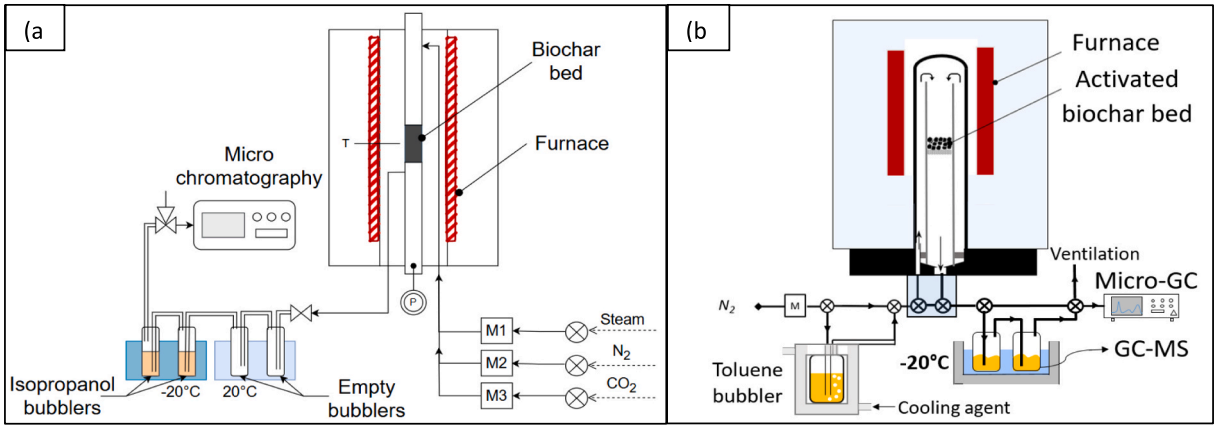

Fig. 1. (a) Biochar activation reactor, (b) Toluene cracking reactor.

The main reactions involved in biochar activation in CO_2 or H_2O atmospheres are, respectively the Boudouard reaction ($C(s) + CO_2 \rightarrow 2CO$) and the steam gasification reaction ($C(s) + H_2O \rightarrow CO + H_2$). Activation under H_2O is significantly faster than activation under CO_2 (Tagutchou et al. 2013). Therefore, the temperature was maintained at 800 °C during H_2O activation and at 900 °C during CO_2 activation. These operating parameters were selected to maintain relatively low gasification kinetics, minimizing the risk of conversion gradients within the biochar sample and ensuring uniform properties across the material.

This challenge of limiting the conversion gradient across the sample, to avoid biochar heterogeneity, also guided our selection of the biochar bed height. With a bed height of approximately 30 mm, resulting in a gas contact time of 0.03 s, we verified that the reactive gas concentration decreased by less than 2 % (by volume) across the bed, ensuring uniform conversion and homogeneous properties throughout the sample.

At the end of each activation test, the gas flow was switched to nitrogen while the furnace cooled to room temperature.

Firstly, tests were carried out to achieve complete conversion of the biochar. The evolution of the conversion rate was determined as a function of time for both activation conditions. Next, tests were carried out to achieve different activation progress by varying the duration of activation. The gasification of the biochar was stopped at different activation progress (Eq. (1) and (2)), namely around 15 %, 25 %, 55 % and 85 %.

Activation progress was calculated using the carbon balance in the gas, based on measurement of CO or CO_2 concentration at the reactor outlet using the sampling train (Fig. 1 (a)). This conversion progress is called X_{gas} and is defined as follows:

$$X_{gas}(\%) = \frac{n_{C,converted,t} \cdot M_C}{m_0 - m_{ash}} \times 100 \quad (1)$$

Where, $n_{C,converted,t}$, M_C, m_0 and m_{ash} are, respectively, the moles of converted carbon at time t, the molar mass of carbon, the initial mass of raw biochar (before activation), and the mass of ash in the raw biochar.

Activation progress was also calculated by weighing the residual biochar at the end of each activation test and comparing it with the initial mass:

$$X(\%) = \frac{m_0 - m_{ab}}{m_0 - m_{ash}} \times 100 \quad (2)$$

Where, m_{ab} is the mass of activated biochar at the end of the test.

2.3. Toluene cracking apparatus

The reactor used for toluene cracking is shown in Fig. 1 (b). It consisted of an outer quartz tube with a diameter of 30 mm and a length of 420 mm, and an inner quartz tube with a diameter of 20 mm and a length of 410 mm. The inner tube was equipped with a fritted disc placed 150 mm from the top of the tube. Both tubes were heated in an electric oven to temperature ranging from 700 to 900 °C. A biochar bed,17 mm in high, was placed on top of the fritted disc. A sufficient flow of gas (>200 Nml/min) was passed through the reactor to ensure adequate contact time with the biochar of about 0.13 s, similar to conditions encountered in industrial reactors.

The gas was first preheated in the annular space between the outer and inner tubes and then further heated in the inner tube before reaching the fixed bed. The residence time of the gas in the isothermal hot zone of the reactor was approximately 6 s. The gas conditioning system consists of a mass flow meter to control the nitrogen flow and a temperature-controlled toluene bubbler. The temperature of the bubbler was set to maintain a toluene concentration of 2400 ppmv in the nitrogen flow.

At the reactor outlet, condensable gases were collected in two bubblers filled with isopropanol which were maintained at −20 °C. The composition of the collected solution was then analysed by GC–MS. Non-condensable gases were continuously monitored using a micro-GC analyser. Preliminary tests allowed to determine that a test duration of 20 min was optimal for studying catalytic cracking before biochar deactivation.

Before and after the cracking test, during cooling, the reactor was flushed by nitrogen to maintain an inert atmosphere. To prevent condensation of toluene and cracking products, the gas lines connecting the toluene bubbler to the condensation system were heated to 250 °C using thermal resistors.

The conversion of toluene was calculated as:

$$X_t(\%) = \frac{m_{t,i} - m_{t,o}}{m_{t,i}} \times 100 \quad (3)$$

where, $m_{t,i}$ is the mass of toluene fed into the reactor and $m_{t,o}$ is the mass of toluene recovered in the isopropanol-filled bubblers at the outlet of the reactor during 20-minute test.

2.4. Biochar characterisation

The samples were dried at 105 °C prior to analysis. The properties of the biochar were characterised using proximate and ultimate analysis, transmission electron microscopy (TEM), nitrogen isotherm sorption at −196 °C and CO_2 isotherm sorption at 0 °C.

2.4.1. Physico-chemical properties

- Moisture content

The moisture content of the biochar was determined in accordance

with the NF EN ISO 18134–3:2015–11 standard, using an air-drying oven set at a temperature of 105 ± 2°C.

- Elemental composition

The elemental composition of the samples was determined according to the EN 15407 standard for carbon (C), hydrogen (H) and nitrogen (N) content using a Flash 2000 Elemental Analyser (Thermo Scientific, USA). Oxygen (O) was determined by difference from C, H, N and ash contents.

- Proximate analysis

Proximate analyses were performed in a muffle furnace according to ISO 562:2010 for volatile matter and EN 15403:2011 for ash content. The fixed carbon content was obtained by difference of ash and volatile matter.

2.4.2. Textural and morphological properties

- Specific surface area and pore size distribution

The specific surface area of raw biochar (i.e., before activation) was measured by CO_2 isotherm adsorption at 0 °C. The Langmuir model (Marsh et Rodríguez-Reinoso 2006) was used for this biochar. For the activated biochars, specific surface area and pore size distributions were determined by nitrogen sorption isotherms at −196 °C. The Brunauer–Emmett–Teller (BET) model was used for these measurements.

In addition, the total pore volume (V_t) was calculated by measuring the liquid volume of the adsorbate (N_2) at a relative pressure of 0.985 atm. The micropores volume (V_{micro}) was estimated using the t-plot method, while the mesopore (V_{meso}) was determined using the Barrett–Joyner–Halenda (BJH) method. The macropores volume (V_{macro}) was calculated by subtracting the micropores and mesopores volumes from the total pore volume.

All measurements were conducted using a 3FLEX analyser (Micromeritics, USA). Prior to each analysis, the samples were outgassed under vacuum at 300 °C for at least 12 h.

- TEM

Transmission electron microscopy (TEM) was employed to image the internal structure and morphology of biochar at the nanoscale (< 100 nm) using a Jeol 2100F (200 kV) microscope.

3. Results and discussion

3.1. Conversion progress of biochars

To control the textural properties of biochars, we conducted experiments in two steps. In a first set of experiments, we achieved complete conversion of the biochars to determine the activation kinetics under CO_2 at 900 °C and H_2O at 800 °C. Then, we produced four activated biochars with different conversion progresses (approximately 15 %, 25 %, 55 % and 85 %) by controlling the duration of activation.

In terms of activation kinetic, Fig. 2 shows the complete biochar conversion (X) as a function of time during CO_2 and H_2O activation at 900 °C and 800 °C respectively (dashed lines, using Eq. (1)). The choice of these temperatures, as explained in the methodology section, was aimed at limiting the activation kinetics to avoid heterogeneous conversion across the biochar bed. Carbon activation kinetics are known to be significantly higher with steam than with CO_2 (Chang, Chang, et Tsai 2000; Van de steene et al. 2011; Teixeira et al. 2012). Note here that activation with CO_2 was 1.8 times faster than with H_2O, primarily due to the difference in activation temperature. In Fig. 2, we observe that up to 90 % conversion, the slopes of the gasification curves for CO_2 and H_2O remained nearly constant. This is consistent with the results of previous studies (Mermoud, Golfier, et al. 2006).

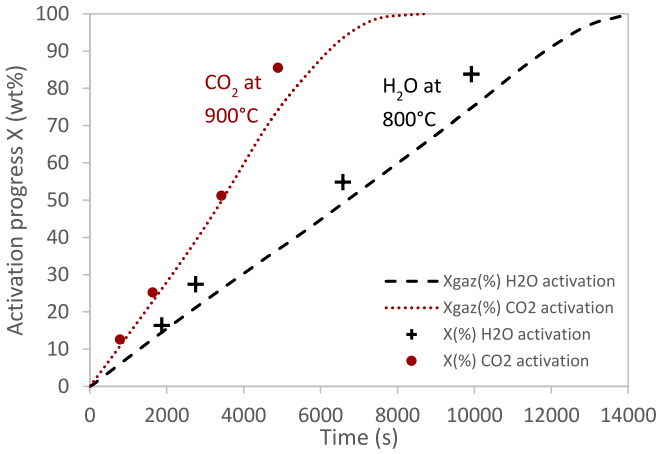

Fig. 2. Activation of biochars in two atmospheres: 900 °C-20 % CO_2 and 800 °C-20 % H_2O.

In Fig. 2, the eight marks correspond to the biochars produced with different conversion times. As previously explained, the conversion progress of each biochar sample was calculated using mass balance approach from Eq. (2). These results are also summarised in Table 2 and compared to those obtained from the complete conversion tests (represented by dashed curves) at each time corresponding to the eight tests. It is worth noting that the relative difference between the two conversion rates did not exceed 20 %. The conversion progress calculated using Eq. (2) was consistently higher than that measured using complete conversion curves. This discrepancy can be attributed to the continuation of the reaction for a short period after switching the gas from reactive to inert in the case of the eight tests at different conversion times.

In the following sections, the eight biochars are named as follows: "*activating agent* − X *conversion progress*". For example, with CO_2 as the activating agent and a conversion progress of 13 %, the biochar is named "CO_2-X13".

3.2. Changes in textural properties

The specific surface area of the raw biochar calculated from the CO_2 adsorption isotherm using the Langmuir model was approximately 295 m^2/g. The textural properties of activated biochar in terms of BET surface area (S_{BET}), micropore surface area (S_{micro}), total pore volume (V_t), micropore volume (V_{micro}), mesopore volume (V_{meso}) and macropore volume (V_{macro}) are listed in Table 3. Repeatability tests of the specific surface area measurements were conducted on biochars activated to 25 % and 55 % under CO_2 and H_2O. The relative error did not exceed 5 %.

The changes in the specific surface area and pore size distribution in the different activated biochars are discussed in the following subsections.

Table 2
Comparison of calculated conversion progress of biochars using the 2 methods.

	X (%)	X_{gas} (%)	Relative error (%)
CO_2 activation at 900 °C	12.6	10.8	14 %
	25.2	23.0	9 %
	51.2	49.7	3 %
	85.5	74.2	13 %
H_2O activation at 800 °C	16.3	14.5	11 %
	27.4	21.9	20 %
	54.8	49.1	10 %
	83.8	74.8	11 %

Table 3
Textural properties of activated biochars.

Sample name	Activation progress (wt%)	Surface area BET S_{BET} (m^2/g)	Micropore surface area S_{micro} (m^2/g)	Pore volume (cm^3/g)			
				Total (V_t)	Micro (V_{micro})	Meso (V_{meso})	Macro (V_{macrp})
	CO_2 activation at 900 °C						
CO_2-X13	13	418	381	0.2309	0.1817	0.0171	0.0322
CO_2-X25	25	582	540	0.3294	0.2423	0.046	0.0466
CO_2-X51	51	757	661	0.4286	0.3143	0.0541	0.0603
CO_2-X86	86	791	659	0.4527	0.3001	0.0719	0.081
	Steam activation at 800 °C						
H_2O-X16	16	437	376	0.2527	0.1787	0.0402	0.0337
H_2O-X27	27	600	452	0.3891	0.2054	0.1358	0.029
H_2O-X55	55	794	432	0.5875	0.1917	0.2836	0.1122
H_2O-X84	84	783	392	0.62	0.1739	0.3349	0.1112

3.2.1. *Specific surface area*

Fig. 3 shows the specific surface area as a function of the activation progress (solid line). The changes in specific surface as a function of activation progress were similar under both activation conditions: CO_2 activation at 900 °C and steam activation at 800 °C. This result is significant because it makes it possible the production of biochars with the same specific surface area but different pore size distributions, allowing this property to be studied independently. Fig. 3 shows that the specific surface area almost doubled during the activation process, from 420 m^2/g for X = 15 % to 775 m^2/g for X = 55 %. Beyond 55 % conversion, the specific surface area remained almost constant up to X = 85 %. This can be explained by the increasing ash content in the biochar during conversion, which, as non-porous material, compensates for the increase in the specific surface area.

To visualize the effect of activation progress on carbon surface area alone, we plotted the ash-free surface area ($S_{af,}$ in m^2/g of activated biochar) (Fig. 3, dashed line). As expected, the ash-free surface area increased almost linearly with the conversion.

However, as the activation progress increased, the available biochar mass decreases even as the surface area increases, due to its consumption during activation. Therefore, a compromise between increasing the surface area and decreasing the mass of biochar needs to be found to determine the activation progress that maximizes the available surface area per gram of raw biochar. The available surface area ($S_{av.}$) is defined in Eq. (4) and plotted as a function of activation progress in Fig. 3 (dashed-dotted line). This surface area corresponds to the available surface per gram of initial biochar (i.e., before activation). The optimum available specific surface area was achieved for an activation progress of approximately 25–30 %. Similar results were obtained by Seo et al. (Seo et al. 2010) with pine wood biochar in a CO_2 atmosphere.

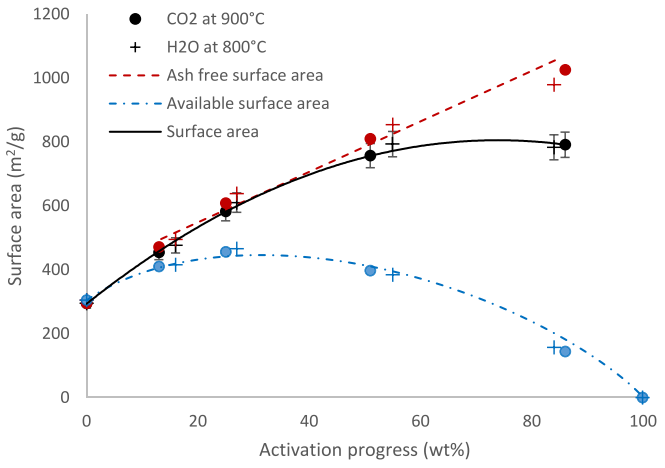

Fig. 3. Changes in the specific surface area with the activation progress during the activation process.

$$S_{av.} = S_{af}(1 - X) \quad (4)$$

3.2.2. *N_2 isotherms and pore size distribution*

The pore sizes of the activated biochars were classified into three groups according to the recommendations of the International Union of Pure and Applied Chemistry (IUPAC): micropores (pore size < 2 nm), mesopores (2–50 nm) and macropores (> 50 nm).

Fig. 4 shows the N_2 sorption isotherms (a and b) and pore size distribution (c and d) of the biochars. The volume of N_2 adsorbed or desorbed increased with the activation progress for all biochars, reflecting increased porosity due to activation reactions. According to Sing et al. (Sing 1985), the isotherms of CO_2 activation (a) are type I, indicating that they are almost microporous (Marsh et Rodríguez-Reinoso 2006; Lowell et Shields 1991). The isotherms of H_2O activation (b) are all type IV except biochar H_2O-X16. The hysteresis observed in these sorption isotherm curves indicates that the samples have a partially mesoporous structure. The hysteresis is of type H4 (Sing 1985) indicating that the pores are slit-shaped (Xu et al. 2020). The isotherm of char H_2O-X16 is type I, reflecting the microporous nature of its structure.

Fig. 4 (c) and (d) show the pore size distributions for CO_2 and H_2O activated biochars, respectively. For CO_2 activation, the pore size was mostly smaller than 2 nm. For H_2O activation, in addition to the pore size smaller than 2 nm (micropores), a significant proportion of the pores ranged from 2 to 10 nm (mesopores).

Fig. 4 (e) shows the changes in the proportions of micro- and mesopores as a function of activation progress. CO_2 activation predominantly resulted in a microporous structure with more than 65 % of the total pore volume, and a small proportion of mesopores, less than 20 %, for all activation progress values. The proportions of micro and mesopore volumes varied slightly as a function of the activation progress. This is consistent with the well-established fact that CO_2 activation typically favours the formation of micropores through reactions such as the Boudouard reaction, which involves the creation of smaller, highly porous structures.

In contrast, during H_2O activation, the proportion of mesopores volume increased significantly (from 15 % for X = 16 % to 55 % for X = 84 %) while the proportion of micropores volume decreased (from 70 % for X = 16 % to 30 % for X = 84 %) with activation progress. This shift on pore structure can be attributed to different mechanisms governing steam activation, which not only creates micropores but also promotes the enlargement and fusion of existing micropores into mesopores. This process of micropore fusion has also been observed by others (Rodríguez-Reinoso et Molina-Sabio 1992).

Furthermore, TEM images (Fig. 5) provide visual evidence of the surface changes when comparing CO_2 and H_2O activation methods. The images for H_2O activation reveal significant surface rearrangement and destruction of the biochar structure comparing to CO_2 activation. The size of the rearranged surface features observed in the TEM images

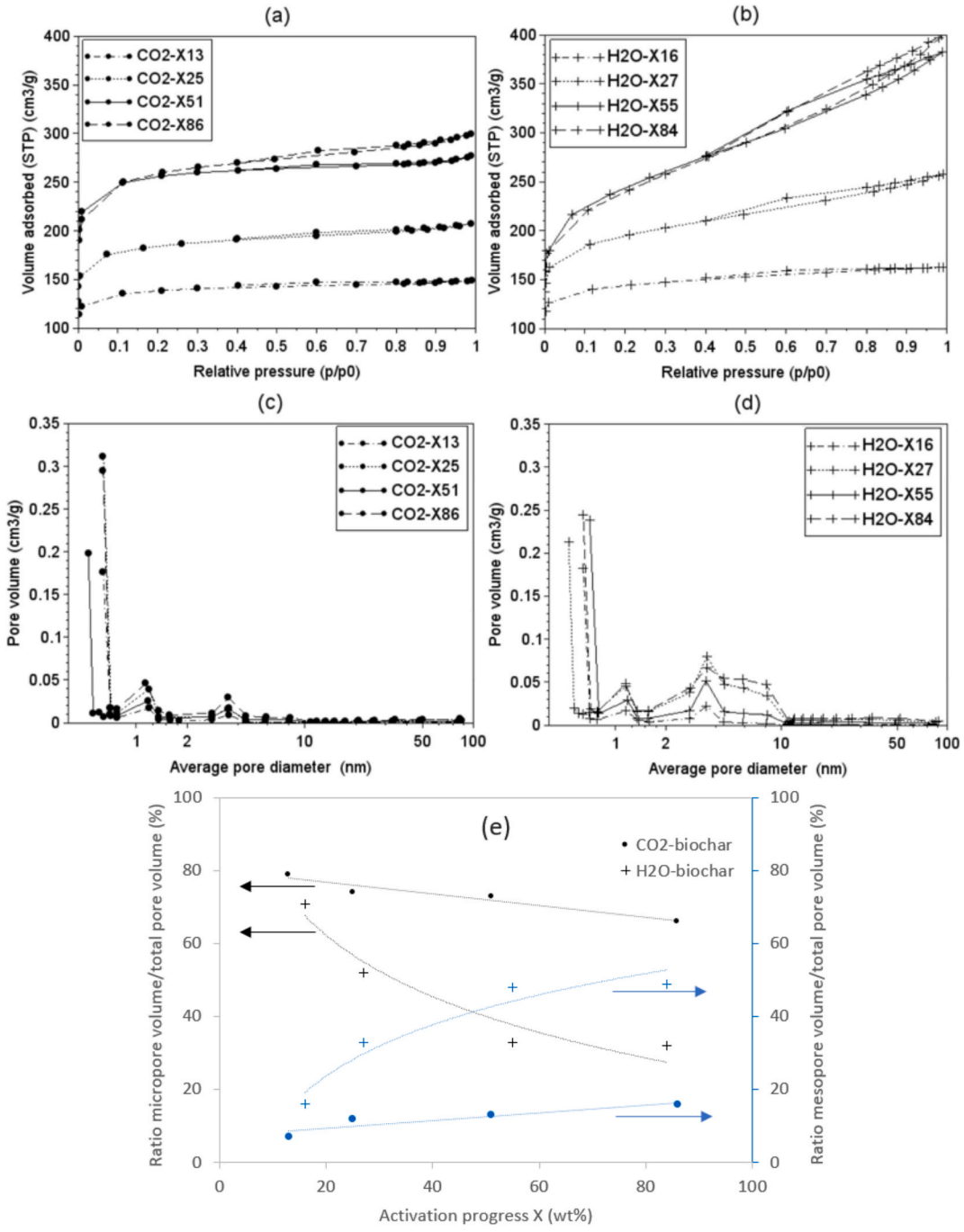

Fig. 4. N_2 sorption isotherms of the CO_2-biochar (a), H_2O-biochar (b) along the conversion, the corresponding pore size distributions for CO_2-biochars (c) and H_2O-biochars (d), and changes in the ratio V_{micro}/V_t and V_{meso}/V_t with the activation progress (e).

corresponds to mesopores, typically in the range of 10 nm. We observed also that the TEM images of raw biochar exhibit a morphology similar to that of CO_2-activated biochar (very fine network), as both materials are predominantly microporous. In contrast, the TEM images of H_2O-activated biochar show a different morphology, characterized by surface cavities at the mesoscale (larger than 2 nm). This observation aligns with previous studies, which demonstrate that the structural modifications induced by steam activation are directly related to the formation of mesoporous structures through the collapse of micropores.

3.3. Tar cracking on biochars

Through the biochar production methodology, we produced biochars with diverse textural structures, which were then used to assess the impact of these structural differences on tar cracking.

Toluene was selected as a model molecule for the cracking test due to its well-established use in similar studies. Cracking tests were performed at two temperatures, 750 °C and 850 °C, with a constant contact time of 0.13 s. By selecting 750 °C and 850 °C, we aimed to operate within a temperature range where the catalytic effects could be more clearly observed and distinguished from homogeneous thermal cracking. These temperatures are lower than those typically used in industrial thermal cracking processes, which can reach up to 1100 °C. Operating at lower temperatures also offers the advantage of reduced energy consumption, making catalytic cracking a more energy-efficient alternative. Each test lasted 20 min, a duration intentionally kept short to minimize biochar

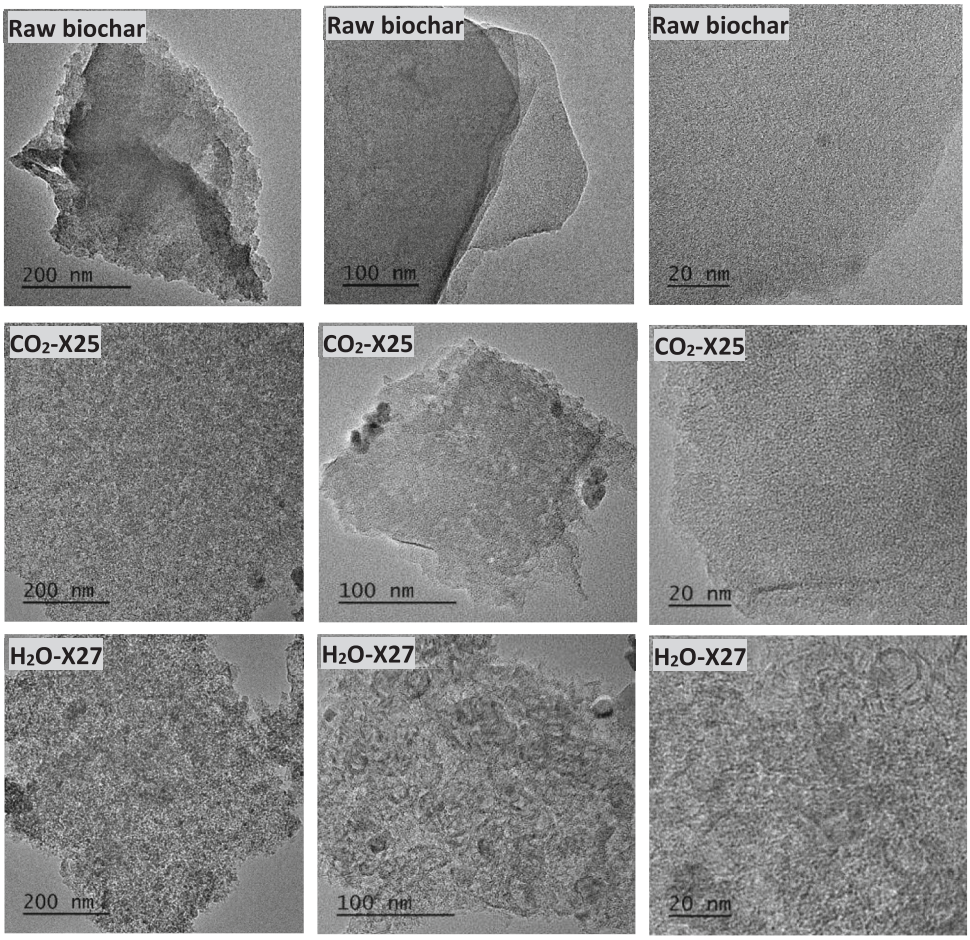

Fig. 5. TEM images of raw biochar and activated biochars at approximately 25% conversion progress are shown, with CO_2 in the middle row and H_2O in the bottom row.

deactivation and ensure the stability of its catalytic activity throughout the process.

The influence of the specific surface area of the biochars on the average toluene conversion rate is shown in Fig. 6. The first data points, corresponding to a specific surface area of 295 m^2/g represent the performance of raw biochar before activation. At 750 °C, the toluene cracking is quite low, around 5 %w.b., while at 850 °C, the conversion increases to 33 %w.b. These conversion progresses are consistent with thermal cracking, as similar results were obtained using inert material such as quartz beads. This suggests that the catalytic effect of the raw biochar on toluene cracking is minimal.

From Fig. 6, it is clear that for both types of activated biochar, under CO_2 and H_2O, the average toluene conversion progress increases with specific surface area. At 850 °C, for specific surface areas greater than 600 m^2/g, the toluene conversion approaches 100 %. However, at 750 °C, even for a biochar with a specific surface area of 800 m^2/g, the conversion rate did not exceed 85 %.

As previously shown, the only differences between the biochars

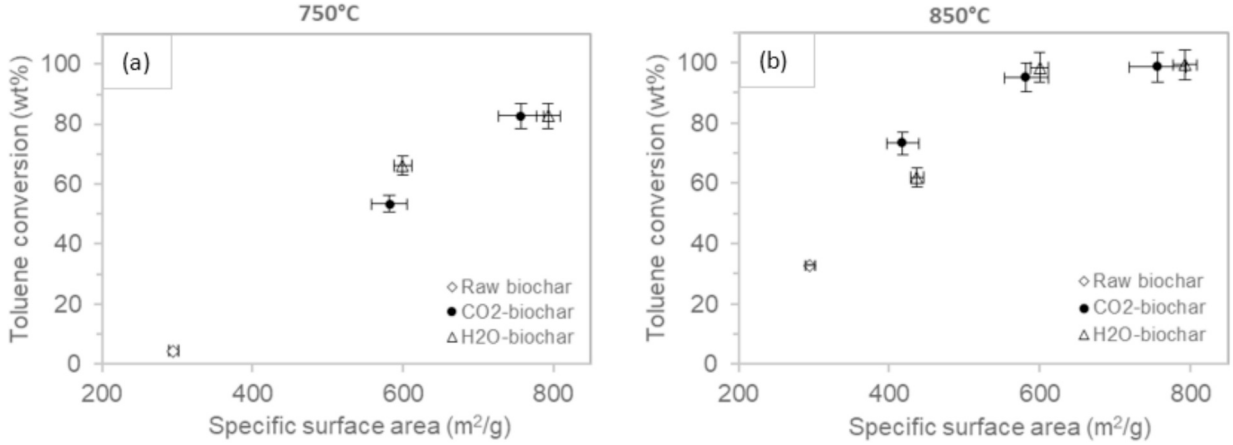

Fig. 6. Average toluene conversion as a function of specific surface area during 20 min catalytic cracking at 750 °C (a) and 850 °C (b).

activated with CO_2 and H_2O are their pore volumes and the distribution between micropores and mesopores. From Fig. 6, it is noteworthy that under our operating conditions, activated biochars produced with either CO_2 or H_2O exhibited similar catalytic activity, with no significant difference in performance. This indicates that pore volume and pore size distribution did not play a substantial role in affecting toluene conversion during 20 min tests.

Next, we focused on the products resulting from toluene cracking and the influence that the textural properties of biochar might have on the nature and distribution of these products. Through sampling and analysis, we were able to establish mass balances for the different cracking experiments; these mass balances are presented in Fig. 7.

The mass balances as a percentage of converted toluene for cracking tests on raw biochars and biochars activated under CO_2 and H_2O, at a conversion rate around 25 %w.b and at temperatures of 750 °C and 850 °C, are shown in Fig. 7. The main products of toluene cracking are coke, benzene (C_6H_6), as well as the following incondensable gases: H_2, CO, CO_2, and CH_4. The presence of oxygen in CO and CO_2 molecules among the products can result in totals exceeding 100 % at specific test points, as this oxygen is sourced from the biochar bed.

At 750 °C, the toluene conversion on raw biochar does not exceed 5 %w.b, meaning that the mass balance for this condition is not reliable and therefore not shown in Fig. 7.

At 850 °C, the mass balance for raw biochar nearly closes 90 %w.b. we observed that the inner surface of the reactor was coated with a layer of dense coke. This part of coke was not taken into account in the mass balance. This may explain the discrepancies in the mass balance. Toluene cracking on this biochar primarily produces another type of tar, benzene (around 40 %w.b), as well as approximately 20 %w.b coke and about 10 %w.b each of H_2, CO, and CO_2.

For activated biochars at 750 °C, whether activated under CO_2 or H_2O, the mass balances are quite similar. They show the following approximate distribution: 60–65 %w.b coke, 10–15 %w.b benzene, 10 %w.b H_2, 6–8 %w.b CO, and less than 5 %w.b CO_2 and CH_4. Upon increasing the temperature to 850 °C, the mass balances results for the activated biochars remain comparable, with some notable changes in products distribution. Specifically, the benzene content drops than more than half, accompanied by a marked decrease in CO_2 and a significant increase in CO (from 10 %w.b to nearly 20 %w.b). This shift can be attributed to the dry reforming reaction of benzene and toluene, which consumes CO_2 and produces more CO and H_2.

When comparing the cracking products from raw and activated biochars, it is clear that activation significantly also enhances the quality of the exit gas. As the specific surface area of the biochars increases, there is a noticeable rise in the production of H_2, CO, and CH_4.

4. Conclusion

Activated biochars from beech wood with different structural properties: specific surface areas and pore size distributions were produced varying activation agent (H_2O or CO_2) atmosphere and activation progress (from 0 to 85 %). Whatever the activation agent, increasing the activation progress increased the specific surface area from 300 to 800 m^2/g. However, the optimum activation progress in terms of total developed surface area was measured between 20 % and 30 % in our activation conditions.

The activating agent mainly affects the nature of the pores created during activation: CO_2 essentially develops micropores, whereas H_2O generates both micro- and mesopores. In addition, under H_2O, the proportion of mesopores increases as the conversion rate increases.

The effect of biochar production conditions was tested in relation to tar cracking application. The selection of activation agent, either H_2O or CO_2, primarily affecting pore size distribution, showed no influence on tar conversion. Conversely, the activation progress, governing the specific surface area, significantly affected tar conversion. At 850 °C, toluene conversion ranged from 35 % for a surface area of 300 m^2/g to around 100 % for a surface are of 800 m^2/g. Furthermore, activation substantially enhances the quality of the exit gas, increasing the concentrations of H_2, CO, and CH_4 as the specific surface area of the biochars increases.

These findings provide valuable insights into the relationship between biochar activation conditions and their structural properties,

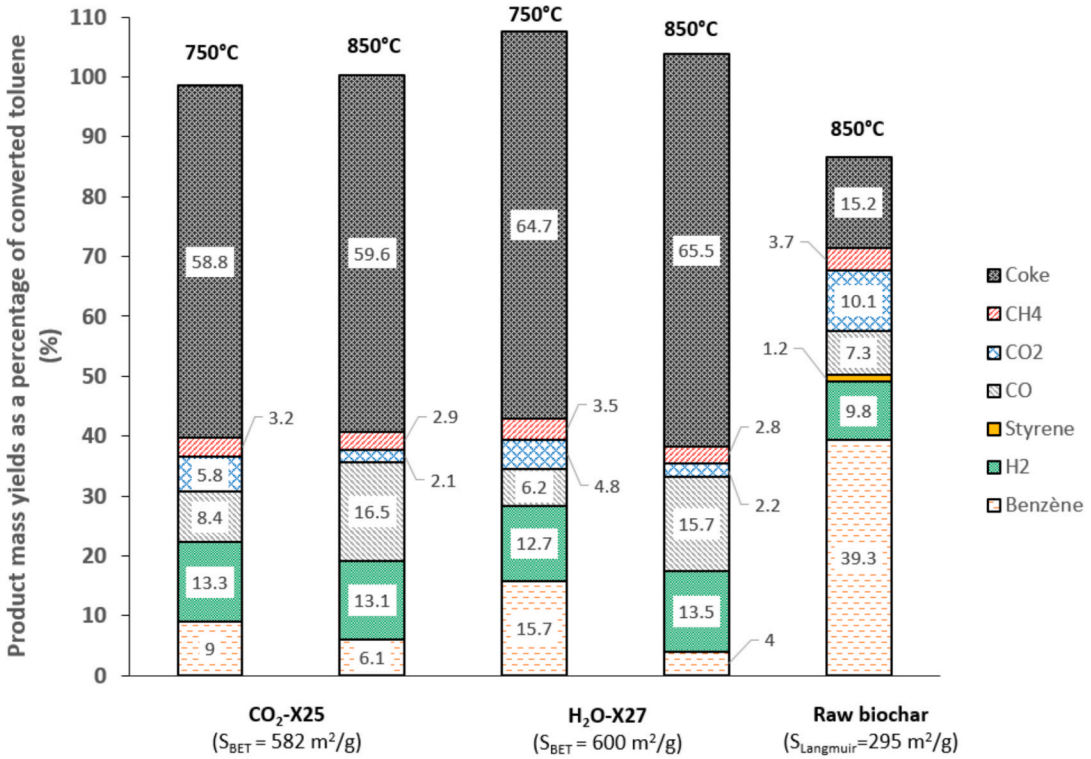

Fig. 7. Mass balances as a percentage of converted toluene during 20 min catalytic cracking at 750 °C and 850 °C.

offering guidance for tailoring biochars for specific industrial applications. Particularly, the results highlight that while activation progress influences tar conversion efficiency, the activation agent mainly determines pore structure, contributing to the optimization of biochar catalysts for applications like tar cracking and gas production.

CRediT authorship contribution statement

Wadii Arayedh: Writing – original draft, Investigation. **Laurent Van de Steene:** Writing – review & editing, Validation, Methodology, Investigation, Conceptualization. **Khashayar Saleh:** Validation, Supervision, Conceptualization. **Elias Daouk:** Writing – review & editing, Validation, Supervision, Investigation.

Declaration of competing interest

The authors declare that they have no known competing financial interests or personal relationships that could have appeared to influence the work reported in this paper.

Acknowledgments

This work was funded by the French Ministry of Higher Education and Research, and CIRAD Montpellier. The authors would like to thank the technicians at the TIMR laboratory, especially Michaël Lefebvre; at the Service of Physico-Chemical Analysis of UTC, especially Caroline Lefebvre and Adama Konate; and at the BioWooEB laboratory, especially Charline Lanvin, Eric Martin, and Jérémy Valette, for their contributions and technical assistance.

Data availability

Data will be made available on request.

References

Bhandari, Pushpak N., Ajay Kumar, Danielle D. Bellmer, et Raymond L. Huhnke. 2014, Synthesis and evaluation of biochar-derived catalysts for removal of toluene (model tar) from biomass-generated producer gas , Renewable Energy 66 (juin):346-53. doi: 10.1016/j.renene.2013.12.017.

Boehm, H.-P., Diehl, E., Heck, W., Sappok, R., 1964. Surface Oxides of Carbon. Angew. Chem. Int. Ed. Eng. 3 (10), 669–677. https://doi.org/10.1002/anie.196406691.

de Caprariis, B., Bassano, C., Bracciale, M.P., Deiana, P., Hernandez, A.D., Santarelli, M. L., Scarsella, M., De Filippis, P., 2020. Biomass Gasification: The Effect of the Surface Area of Different Materials on Tar Abatement Efficiency. Energy Fuel 34 (2), 1137–1144. https://doi.org/10.1021/acs.energyfuels.9b02371.

Chang, C.-F., Chang, C.-Y., Tsai, W.-T., 2000. Effects of Burn-off and Activation Temperature on Preparation of Activated Carbon from Corn Cob Agrowaste by CO2 and Steam. Journal of Colloid and Interface Science 232 (1), 45–49. https://doi.org/10.1006/jcis.2000.7171.

Coll, R., Salvadó, J., Farriol, X., Montané, D., 2001. Steam reforming model compounds of biomass gasification tars: conversion at different operating conditions and tendency towards coke formation. Fuel Process. Technol. 74 (1), 19–31. https://doi.org/10.1016/S0378-3820(01)00214-4.

Dhawane, Sumit H., et Gopinath Halder. 2019, Chapter 11 - Synthesis of Catalyst Support From Waste Biomass for Impregnation of Catalysts in Biofuel Production , In Advances in Feedstock Conversion Technologies for Alternative Fuels and Bioproducts, édité par Majid Hosseini, 199-220. Woodhead Publishing Series in Energy. Woodhead Publishing. doi: 10.1016/B978-0-12-817937-6.00011-4.

Dufourny, A., Van De Steene, L., Humbert, G., Guibal, D., Martin, L., Blin, J., 2019. Influence of pyrolysis conditions and the nature of the wood on the quality of charcoal as a reducing agent. J. Anal. Appl. Pyrol. 137 (janvier):1–13. https://doi.org/10.1016/j.jaap.2018.10.013.

Fuentes-Cano, Diego, Alberto Gómez-Barea, Susanna Nilsson, et Pedro Ollero. 2013, Decomposition kinetics of model tar compounds over chars with different internal structure to model hot tar removal in biomass gasification , Chemical Engineering Journal 228 (juillet):1223-33. doi: 10.1016/j.cej.2013.03.130.

Hazmi, B., Rashid, U., Akhlisah, Z.N., Chaowamalee, S., Ngamcharussrivichai, C., Sabater, M.J., 2025. Productive esterification of palm fatty acid distillate under lignocellulosic biomass char of rambutan seeds waste-supported sulfonated catalyst. Biomass Bioenergy 194 (mars), 107607. https://doi.org/10.1016/j.biombioe.2025.107607.

Henriksen, U., Hindsgaul, C., Qvale, B., Fjellerup, J., Jensen, A.D., 2006. Investigation of the Anisotropic Behavior of Wood Char Particles during Gasification. Energy Fuel 20 (5), 2233–3228. https://doi.org/10.1021/ef060140f.

Hilber, I., Bucheli, T., 2013. Activated carbon amendment to remediate contaminated sediments and soils: a review. Global NEST Journal 12 (3), 305–317. https://doi.org/10.30955/gnj.000723.

Huchon, V., Martin, E., Pinta, F., Commandré, J.M., L. Van de steene, 2024. Conversion in a char bed reactor of tars and syngas from a wood gasifier. Energy 288 (février), 129738. https://doi.org/10.1016/j.energy.2023.129738.

İnan, B., Koçer, A.T., Özçimen, D.B., 2023. Valorization of lignocellulosic wastes for low-cost and sustainable algal biodiesel production using biochar-based solid acid catalyst. J. Anal. Appl. Pyrol. 173 (août), 106095. https://doi.org/10.1016/j.jaap.2023.106095.

Iwanow, M., Gärtner, T., Sieber, V., König, B., 2020. Activated Carbon as Catalyst Support: Precursors, Preparation, Modification and Characterization. Beilstein J. Org. Chem. 16 (1), 1188–1202. https://doi.org/10.3762/bjoc.16.104.

Korus, A., Samson, A., Szlęk, A., 2020. Catalytic conversion of toluene over a biochar bed under an inert atmosphere – The comparison of chars from different types of wood and the role of selected metals. Fuel 279 (novembre), 118468. https://doi.org/10.1016/j.fuel.2020.118468.

Lowell, S., et Joan E. Shields. 1991. Powder Surface Area and Porosity. Springer Netherlands. http://link.springer.com/10.1007/978-94-015-7955-1.

Marsh, Harry, et Francisco Rodríguez-Reinoso. 2006, CHAPTER 4 - Characterization of Activated Carbon , In Activated Carbon, édité par Harry Marsh et Francisco Rodríguez-Reinoso, 143-242. Oxford: Elsevier Science Ltd. doi: 10.1016/B978-008044463-5/50018-2.

Mermoud, F., Golfier, F., Salvador, S., Van de Steene, L., Dirion, J.L., 2006a. Experimental and Numerical Study of Steam Gasification of a Single Charcoal Particle. Combust. Flame 145 (1), 59–79. https://doi.org/10.1016/j.combustflame.2005.12.004.

Mermoud, F., Salvador, S., Van de Steene, L., Golfier, F., 2006b. Influence of the Pyrolysis Heating Rate on the Steam Gasification Rate of Large Wood Char Particles. Fuel 85 (10), 1473–1482. https://doi.org/10.1016/j.fuel.2005.12.004.

Milne, T. A., R. J. Evans, et N. Abatzaglou. 1998, Biomass Gasifier "Tars": Their Nature, Formation, and Conversion , NREL/TP-570-25357; ON: DE00003726. National Renewable Energy Laboratory, Golden, CO (US). doi: 10.2172/3726.

Mohamed, A.R., Mohammadi, M., Darzi, G.N., 2010. Preparation of Carbon Molecular Sieve from Lignocellulosic Biomass: A Review. Renew. Sustain. Energy Rev. 14 (6), 1591–11159. https://doi.org/10.1016/j.rser.2010.01.024.

Nestler, F., Burhenne, L., Amtenbrink, M., Aicher, T., 2016. Catalytic decomposition of biomass tars: The impact of wood char surface characteristics on the catalytic performance for naphthalene removal. Fuel Process. Technol. 145 (mai):31–41. https://doi.org/10.1016/j.fuproc.2016.01.020.

Pattanotai, T., Watanabe, H., Okazaki, K., 2013. Experimental Investigation of Intraparticle Secondary Reactions of Tar during Wood Pyrolysis , Fuel, 10th Japan/China Symposium on Coal and C1. Chemistry 104 (février):468–75. https://doi.org/10.1016/j.fuel.2012.08.047.

Rodríguez-Reinoso, F., Molina-Sabio, M., 1992. Activated Carbons from Lignocellulosic Materials by Chemical and/or Physical Activation: An Overview. Carbon 30 (7), 1111–1118. https://doi.org/10.1016/0008-6223(92)90143-K.

Seo, Dong Kyun, Sun Ki Lee, Min Woong Kang, Jungho Hwang, et Tae-U. Yu. 2010, Gasification Reactivity of Biomass Chars with CO2 , Biomass and Bioenergy, Current and Potential Capabilities of Wood Production Systems in the Southeastern U.S., 34 (12): 1946-53. doi: 10.1016/j.biombioe.2010.08.008.

Shen, Y., Yoshikawa, K., 2013. Recent progresses in catalytic tar elimination during biomass gasification or pyrolysis—A review. Renewable and Sustainable Energy Reviews 21 (mai):371–92. https://doi.org/10.1016/j.rser.2012.12.062.

Sing, K.S.W., 1985. Reporting Physisorption Data for Gas/Solid Systems with Special Reference to the Determination of Surface Area and Porosity (Recommendations 1984). Pure Appl. Chem. 57 (4), 603–619. https://doi.org/10.1351/pac198557040603.

Tagutchou, J. P., L. Van de steene, F. J. Escudero Sanz, et S. Salvador. 2013, Gasification of Wood Char in Single and Mixed Atmospheres of H2O and CO2 , Energy Sources, Part A: Recovery, Utilization, and Environmental Effects 35 (13): 1266-76. doi: 10.1080/15567036.2010.542438.

Teixeira, G., L. Van de Steene, E. Martin, F. Gelix, et S. Salvador. 2012, Gasification of char from wood pellets and from wood chips: Textural properties and thermochemical conversion along a continuous fixed bed , Fuel, Special Section: ACS Clean Coal, 102 (décembre):514-24. doi: 10.1016/j.fuel.2012.05.039.

Van de steene, L., J. P. Tagutchou, F. J. Escudero Sanz, et S. Salvador, 2011. Gasification of Woodchip Particles: Experimental and Numerical Study of Char–H2O, Char–CO2, and Char–O2 Reactions. Chem. Eng. Sci. 66 (20), 4499–4509. https://doi.org/10.1016/j.ces.2011.05.045.

Wang, Fang-Jie, Shu Zhang, Zong-Ding Chen, Chen Liu, et Yong-Gang Wang. 2014, Tar reforming using char as catalyst during pyrolysis and gasification of Shengli brown coal , Journal of Analytical and Applied Pyrolysis 105 (janvier):269-75. doi: 10.1016/j.jaap.2013.11.013.

Wong, Syieluing, Norzita Ngadi, Ibrahim M. Inuwa, et Onn Hassan. 2018, Recent Advances in Applications of Activated Carbon from Biowaste for Wastewater Treatment: A Short Review , Journal of Cleaner Production 175 (février):361-75. doi: 10.1016/j.jclepro.2017.12.059.

Xu, Longfei, Yiyi Zhang, James Ding, Liu, Yong Shi, Zhenwang Li, Yudong Dang, Nai-Chen Cheng, et Baosu Guo. 2020, Pore Structure and Fractal Characteristics of Different Shale Lithofacies in the Dalong Formation in the Western Area of the Lower Yangtze Platform , Minerals 10 (janvier):72. doi: 10.3390/min10010072.